

Cosmic Microwave Background Acoustic Peak Locations

Z. Pan,^{1*} L. Knox,^{1†} B. Mulroe,^{2‡} A. Narimani,^{3§}

¹*Department of Physics, University of California, One Shields Avenue, Davis, CA, USA 95616*

²*Department of Physics, Fordham University, 441 East Fordham Road, Bronx, NY, USA 10458*

³*Department of Physics & Astronomy, University of British Columbia, 6224 Agricultural Road, Vancouver, BC, V6T 1Z1 Canada*

7 April 2016

ABSTRACT

The *Planck* collaboration has measured the temperature and polarization of the cosmic microwave background well enough to determine the locations of eight peaks in the temperature (TT) power spectrum, five peaks in the polarization (EE) power spectrum and twelve extrema in the cross (TE) power spectrum. The relative locations of these extrema give a striking, and beautiful, demonstration of what we expect from acoustic oscillations in the plasma; e.g., that EE peaks fall half way between TT peaks. We expect this because the temperature map is predominantly sourced by temperature variations in the last scattering surface, while the polarization map is predominantly sourced by gradients in the velocity field, and the harmonic oscillations have temperature and velocity 90 degrees out of phase. However, there are large differences in expectations for extrema locations from simple analytic models vs. numerical calculations. Here we quantitatively explore the origin of these differences in gravitational potential transients, neutrino free-streaming, the breakdown of tight coupling, the shape of the primordial power spectrum, details of the geometric projection from three to two dimensions, and the thickness of the last scattering surface. We also compare the peak locations determined from *Planck* measurements to expectations under the Λ CDM model. Taking into account how the peak locations were determined, we find them to be in agreement.

Key words: cosmic microwave background – cosmology: theory

1 INTRODUCTION

With the first release of *Planck* polarization data (Planck Collaboration XI 2015; Planck Collaboration XIII 2015) we have for the first time a sufficient measurement of the polarization spectra (both the temperature-E-mode polarization cross power spectrum (TE) and the E-mode auto power spectrum (EE)) to clearly see multiple acoustic peaks with well-defined locations. These locations provide a beautiful confirmation of expectations for the response of the primordial plasma to small initial adiabatic departures from complete homogeneity.

One can work out these expectations by solving the Einstein-Boltzmann equations for evolution of the phase space distribution function of the various components (e.g. Mukhanov 1992; Ma & Bertschinger 1995; Seljak & Zaldarriaga 1996; Lewis et al. 2000; Lesgourgues & Tram 2011). But these numerical calculations, on their own, are not en-

tirely satisfying. In addition to knowing the answer, we want understanding. This desire has led to many papers aimed at an analytic understanding of the model power spectra (e.g. Peebles & Yu 1970; Doroshkevich et al. 1978; Atrio-Barandela & Doroshkevich 1994; Seljak 1994; Jorgensen et al. 1995; Hu & Sugiyama 1994, 1995, 1996; Hu & White 1996; Zaldarriaga & Harari 1995; Hu & White 1997b; Weinberg 2001a,b, 2002; Mukhanov 2004; Bartolo et al. 2007; Cai & Zhang 2012). In this article, motivated by the recent first measurements of TE and EE extrema locations, we develop a detailed analytic understanding of the locations of the peaks in TT and EE, and the extrema in TE in the context of Λ CDM model.

The peak structure itself has drawn special attention. Back to about 15 years ago, when only the first TT peak was readily measured (e.g. Scott & White 1994; Smoot & Scott 1997; Hancock et al. 1998; Lineweaver & Barbosa 1998; Bond et al. 1998, 1999; Bond & H. Jaffe 1999; Miller et al. 1999; Efstathiou et al. 1999; Tegmark 1999; Tegmark & Zaldarriaga 2000b,a; Bond et al. 2000b,a; Knox & Page 2000; Bernardis et al. 2000; Pierpaoli 2000), it was found to be consistent with the standard Λ CDM model with adiabatic initial conditions, and imposed tight constraints on other

* Email: zhpan@ucdavis.edu

† Email: lknox@ucdavis.edu

‡ Email: bmulroe@fordham.edu

§ Email: anariman@phas.ubc.ca

competing models for example, Λ CDM model with isocurvature initial conditions and topological defect models (e.g. [Hu & Sugiyama 1995](#); [Turok 1996a,b](#); [Magueijo et al. 1996](#)). With more peaks measured in recent years ([Jaffe et al. 2001](#); [Bernardis et al. 2002](#); [Page et al. 2003](#); [Benoît et al. 2003](#); [Durrer et al. 2001](#); [Readhead et al. 2004](#); [Jones et al. 2006](#); [Hinshaw et al. 2007](#); [Corasaniti & Melchiorri 2008](#); [Pryke et al. 2008](#); [Naess et al. 2014](#)), the topological defect models were ruled out ([Albrecht 2000](#)), and the constraints on the isocurvature modes have been improved to unprecedented precision (e.g. [Bucher et al. 2001](#); [Trotta et al. 2001](#); [Amen-dola et al. 2002](#); [Bucher et al. 2002](#); [Moodley et al. 2004](#); [Bean et al. 2006](#); [Komatsu et al. 2009, 2011](#); [Hinshaw et al. 2013](#); [Planck Collaboration XXII 2014](#)).

Part of the beauty of the TT, TE and EE measurements is that a very simple analytic model provides us with a qualitative understanding of the observed features. In the next section we will define this model and use it to produce ‘baseline’ predictions for the peak locations. It works especially well for the relative locations of the peaks. For example, the temperature anisotropies are predominantly sourced by temperature fluctuations at the last scattering surface (LSS). We expect that the standing-wave modes that have hit an extremum in temperature contrast right at the epoch of last scattering, will be at a null in their peculiar velocities. Further, since gradients in peculiar velocities are the dominant source of polarization anisotropy, peaks in TT should correspond to minima in EE. This is roughly what we observe.

But the above picture is discrepant, in detail, with observations and with the expectations of the Λ CDM model. To achieve an understanding that is quantitatively correct, at a level consistent with the precision of current measurements, we have to take into account a number of effects. We have found that all these factors are important: time-varying gravitational potentials that are still non-zero at last scattering, neutrino free-streaming, the failure of the tight-coupling approximation, the shape of the primordial power spectrum, details of the projection from three dimensions to two, and the finite width of the LSS. We work out, sometimes analytically, mostly by numerical methods, the contribution of each one of these effects to the shifting of each of the peaks from their locations in the baseline model.

The paper is organized as follows. In Section 2, we introduce a baseline model interpreting the evolution of photon perturbations and the power spectra based on the tight coupling approximation and simplified projection. In Section 3, we first analytically derive the phase shifts of photon perturbations induced by decoupling, gravitational potential transient and free-streaming neutrinos, then numerically test the analytic results by examining the evolution of a single k mode. In Section 4, we numerically measure the phase shift of the photon perturbations at the LSS, single out the contribution from each effect, and analytically interpret them. In Section 5, we investigate the impact of projection on the peak locations in details. We compare the peak locations determined from *Planck* measurements to expectations under the Λ CDM model in Section 6, and conclude in Section 7.

In this paper, we will work in the conformal Newtonian gauge

$$ds^2 = a^2(\eta) \left[-(1 + 2\Phi)d\eta^2 + (1 - 2\Psi)\delta_{ij}dx^i dx^j \right], \quad (1)$$

where η is the conformal time, and the scalar perturbation Ψ and Φ are related to the convention of [Dodelson \(2003\)](#) by $\Phi = \Psi_{\text{Dodelson}}$, $\Psi = -\Phi_{\text{Dodelson}}$. The fiducial cosmology used in the paper is the best fitting flat Λ CDM cosmology from *Planck* TT+low P+lensing ([Planck Collaboration XIII 2015](#)).

2 BASELINE MODEL

In this section, we will construct a simple analytic model, our baseline model, that predicts the peak locations. This simple model neglects many important effects. Much of the rest of the paper is then devoted to explaining the differences between the approximate predictions of this baseline model, and the numerically calculated, essentially exact predictions.

2.1 Before Recombination

The evolution of a photon-baryon plasma is governed by the Einstein-Boltzmann equations, e.g., Eqs.(4.100 - 4.107) of [Dodelson \(2003\)](#),

$$\Theta - \Theta_0 - \mu V_b + \frac{\Pi}{2} P_2(\mu) = \frac{\dot{\Theta} - \dot{\Psi} + ik\mu(\Theta + \Phi)}{\dot{\tau}}, \quad (2)$$

$$\Theta_p - \frac{\Pi}{2} (1 - P_2(\mu)) = \frac{\dot{\Theta}_p + ik\mu\Theta_p}{\dot{\tau}}, \quad (3)$$

$$V_b + 3i\Theta_1 = \frac{R_b \left(\dot{V}_b + \frac{\dot{a}}{a} V_b + ik\Phi \right)}{\dot{\tau}}, \quad (4)$$

where V_b is the bulk velocity of baryons, Θ_p is the strength of the polarization field, $\Pi = \Theta_2 + \Theta_{p2} + \Theta_{p0}$, $\tau(\eta)$ is the optical depth for a photon emitted at time η and received at today η_0 , $R_b (= 3\rho_b/4\rho_\gamma)$ is roughly the ratio of baryon density over photon density, the dot denotes the derivative with respect to the conformal time η , and $\mu = \hat{k} \cdot \hat{p}$ is the cosine of the angle subtended by the wavevector \vec{k} and the photon propagation direction \vec{p} . To be clear, we adopt the most commonly used convention of Legendre multipoles, $\Theta(\mu) = \sum_{\ell=0}^{\infty} (-i)^\ell (2\ell + 1) \Theta_\ell P_\ell(\mu)$ in Eq. (4), and we neglect the small corrections induced by the nonzero sound speed of baryons $c_b^2 \sim T_b/\mu_b$, where T_b is the temperature of baryons and μ_b is the mean molecular weight (see e.g. [Ma & Bertschinger 1995](#), for details).

In the tight coupling limit, the first few multipoles can be obtained by perturbative expansion with respect to $k/\dot{\tau}$, which is expected to be much smaller than unity before decoupling. Expanding Eqs. (2-4) to $O(k/\dot{\tau})$, we get (also see [Hu & Sugiyama 1994, 1995, 1996](#); [Hu & White 1996](#); [Zaldarriaga & Harari 1995](#); [Seljak & Zaldarriaga 1996](#))

$$\Pi = \frac{5}{2} \Theta_2, \Theta_2 = -\frac{8}{15} \frac{k}{\dot{\tau}} \Theta_1, \Theta_1 = \frac{i}{k} \left(\dot{\Theta}_0 - \dot{\Psi} \right), \quad (5)$$

and the monopole satisfies

$$\left\{ \frac{d^2}{d\eta^2} + k^2 c_s^2 \right\} [\Theta_0 - \Psi] = -\frac{k^2}{3} (\Phi + \Psi), \quad (6)$$

where $c_s = 1/\sqrt{3(1 + R_b)}$ is the sound speed of the photon-baryon plasma and we have dropped a small correction $\sim R_b$ in the above equation. The monopole is actually a simple harmonic oscillator forced by gravitational driving. Potentials Φ and Ψ decay rapidly inside horizon during radiation

domination, and keep constant during matter domination. For simplicity we drop, for now, the $\dot{\Psi}$ term on the left side of the above equation and we have (Hu & Dodelson 2002)

$$\left\{ \frac{d^2}{d\eta^2} + k^2 c_s^2 \right\} [\Theta_0 + \Phi] = 0, \quad (7)$$

where we have used the facts that $\Phi = \Psi$ in the absence of photon anisotropic stress, $c_s^2 \simeq 1/3$, and $\dot{\Psi}$ term is small after potentials decay. Assuming adiabatic initial conditions, expected from the simplest inflationary models, $[\dot{\Theta} + \dot{\Phi}](\eta = 0) = 0$, we obtain

$$[\Theta_0 + \Phi] \propto \cos(kr_s), \quad \Theta_1 \propto \sin(kr_s), \quad \Pi \propto \frac{k}{\dot{\tau}} \sin(kr_s), \quad (8)$$

where $r_s(\eta) = \int_0^\eta c_s d\eta$ is the sound horizon at time η .

2.2 After Recombination

After recombination, photons freely stream. Hence the temperature anisotropies we observed today are largely determined by the photon perturbation at the LSS, $\Theta(\vec{x} = 0, \hat{\gamma}, \eta = \eta_0) \simeq [\Theta_0 + \Phi](\vec{x} = \hat{\gamma}(\eta_0 - \eta_*) , \hat{\gamma}, \eta = \eta_*)$,¹ where $\hat{\gamma}$ is the observation direction, η_0 is the conformal time today and η_* is the conformal time of the LSS. To study the statistical property of the anisotropies, we usually expand the field in terms of spherical harmonics

$$a_{\ell m} = \int d\Omega Y_{\ell m}(\hat{\gamma}) \Theta(\vec{x} = 0, \hat{\gamma}, \eta = \eta_0), \quad (9)$$

and define the temperature power spectrum $C_\ell^{\text{TT}} \equiv \langle a_{\ell m} a_{\ell m}^* \rangle$. With some geometric transforms (e.g. Dodelson 2003), the power spectrum is explicitly expressed as

$$C_\ell^{\text{TT}} = \int dk k^2 \Theta_\ell^2(k), \quad (10)$$

where $\Theta_\ell(k)$ is the multipole moment of the temperature field of \vec{k} mode,

$$\Theta_\ell(k) = \frac{1}{(-i)^\ell} \int_{-1}^1 \frac{d\mu}{2} P_\ell(\mu) \Theta(\vec{k}, \hat{\gamma}, \eta_0), \quad (11)$$

where $\mu = \hat{k} \cdot \hat{\gamma}$.

Using the plane-wave pattern (see Fig. 5)

$$\begin{aligned} \Theta(\vec{k}, \hat{\gamma}, \eta_0) &\simeq [\Theta_0 + \Phi](\vec{k}, \hat{\gamma}, \eta_*) \\ &= [\Theta_0 + \Phi](k, \eta_*) \times e^{i\hat{\gamma} \cdot \vec{k}(\eta_0 - \eta_*)}, \end{aligned} \quad (12)$$

where $[\Theta_0 + \Phi](k, \eta_*)$ is the oscillation amplitude [Eq. (8)] and $e^{i\hat{\gamma} \cdot \vec{k}(\eta_0 - \eta_*)}$ is the spatial pattern, we have

$$\begin{aligned} \Theta_\ell(k) &\simeq \frac{1}{(-i)^\ell} \int_{-1}^1 \frac{d\mu}{2} P_\ell(\mu) [\Theta_0 + \Phi](k, \eta_*) e^{i\mu k(\eta_0 - \eta_*)}, \\ &= (-1)^\ell [\Theta_0 + \Phi](k, \eta_*) j_\ell[k(\eta_0 - \eta_*)], \end{aligned} \quad (13)$$

where $j_\ell[k(\eta_0 - \eta_*)]$ is a spherical Bessel function, which peaks at $\ell \simeq k(\eta_0 - \eta_*)$. Therefore, we expect the TT power at mode ℓ is mainly sourced by $[\Theta_0 + \Phi](k, \eta_*)$ by mode $k \simeq \ell/(\eta_0 - \eta_*)$. Similar argument yields that EE and TE

¹ Strictly speaking, it is more appropriate to write $[\Theta + \Phi](\vec{x} = 0, \hat{\gamma}, \eta = \eta_0) \simeq [\Theta_0 + \Phi](\vec{x} = \hat{\gamma}(\eta_0 - \eta_*), \hat{\gamma}, \eta = \eta_*)$, but the local potential today $\Phi(\vec{x} = 0, \eta = \eta_0)$ has no direction dependence, thus has no influence on the CMB anisotropies.

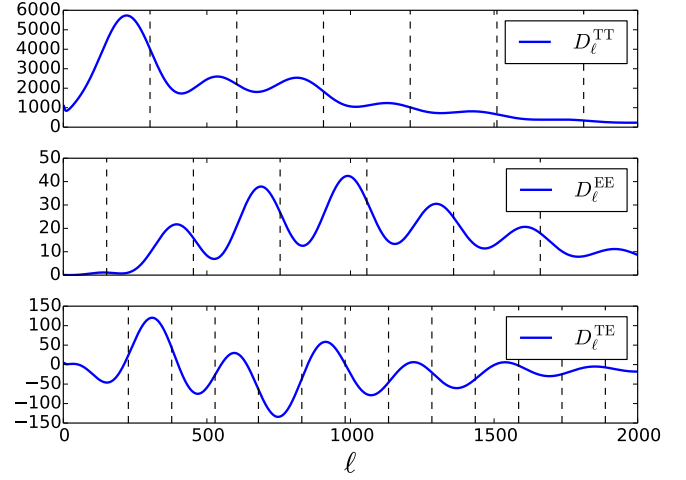


Figure 1. Comparison of the spectra of the fiducial cosmology (solid curves) and the peak locations predicted by the baseline model (vertical dashed lines).

are mainly sourced by $\Pi(k, \eta_*)$ and $[(\Theta_0 + \Phi) \times \Pi](k, \eta_*)$, respectively (see e.g. Hu & Sugiyama 1995; Zaldarriaga & Harari 1995; Hu & White 1997a; Tram & Lesgourgues 2013). As a result,

$$\begin{aligned} D_\ell^{\text{TT}} &\sim [\Theta_0 + \Phi]^2(kr_{s,*}) \propto \cos^2(\ell\theta_*), \\ D_\ell^{\text{EE}} &\sim \Pi^2(kr_{s,*}) \propto \sin^2(\ell\theta_*), \\ D_\ell^{\text{TE}} &\sim \{[\Theta_0 + \Phi] \times \Pi\}(kr_{s,*}) \propto \sin(2\ell\theta_*), \end{aligned} \quad (14)$$

where $D_\ell^{\text{XX}} \equiv \ell(\ell + 1)/(2\pi)C_\ell^{\text{XX}}$, with $\text{XX} = \text{TT}, \text{TE}, \text{EE}$, and θ_* is the angular size of the sound horizon at recombination, $\theta_* \equiv r_{s,*}/(\eta_0 - \eta_*) = 1.04 \times 10^{-2}$ (e.g. Planck Collaboration XVI 2014; Planck Collaboration XIII 2015). Therefore $D_\ell^{\text{TT}}, D_\ell^{\text{EE}}, D_\ell^{\text{TE}}$ reach their p -th peak at

$$\begin{aligned} \ell_p^0(\text{TT}) &= 302 p, \\ \ell_p^0(\text{EE}) &= 302(p - 0.5), \\ \ell_p^0(\text{TE}) &= 151(p + 0.5), \end{aligned} \quad (15)$$

respectively (Throughout this paper, we refer to both the *maxima* and the *minima* in the TE power spectrum as *peaks* due to the arbitrary sign of E mode, and we also refer to the zero points of the TE power spectrum as *troughs*). We are only interested in the peaks in the power spectra which correspond to the extrema of sources $[\Theta_0 + \Phi]$, Π , $[\Theta_0 + \Phi] \times \Pi$, and so carry phase information of the acoustic oscillation. The troughs in the spectra corresponding to the zero points of the sources also carry phase information, but baryon drag shifts the zero points and introduces extra uncertainty. Therefore the troughs in the spectra, and the reionization bumps in EE and TE power spectra are not investigated in this paper.

In Fig. 1, we compare the theoretical spectra of the fiducial cosmology with the baseline model. The baseline model is roughly correct in its prediction for peak spacing and for the relative locations of the peaks in different spectra. But peak locations predicted by the baseline model do not coincide with the true locations, and the typical phase shift $\delta\ell_p$ is about one fourth of the oscillation period. In addition, the baseline model also predicts that EE peaks are located

halfway between TT peaks and also halfway between TE peaks, which is not exactly true either.

Despite its deficiencies, we find the baseline model to be a useful starting point. In the remainder of the paper we explain the differences between these baseline predictions and the predictions of the Λ CDM model when calculated much more precisely.

3 EVOLUTION OF PHASE SHIFTS IN THE PHOTON PERTURBATIONS

According to the baseline model, $\Theta_0(\Theta_1)$ can be described as a simple harmonic oscillator under two assumptions: tight coupling between photons and baryons, and negligible impact of gravitational driving. In fact, both the decoupling effect and decaying gravitational potentials affect the amplitude and the phase of the acoustic oscillation. Taking these into account, we may formally write the solution as

$$[\Theta_0 + \Phi] \propto \cos(kr_s + \phi_{\text{tot}}), \quad (16)$$

where $\phi_{\text{tot}} \equiv \phi_{\text{dcp}} + \phi_{\text{gr}}$ with $\phi_{\text{dcp}}, \phi_{\text{gr}}$ denoting the phase shift induced by decoupling and gravitational driving, respectively. The latter can be further decomposed as $\phi_{\text{gr}} = \phi_{\text{gr},\gamma} + \phi_{\text{gr},\nu}$, due to the fact that the decay of $\Phi + \Psi$ is caused by photon pressure and neutrino free-streaming. To distinguish them, we call $\phi_{\text{gr},\gamma}$ as gravitational potential transient induced phase shift, and call $\phi_{\text{gr},\nu}$ as neutrino induced phase shift. The reason for this decomposition shall be clear later.

In the remainder of this section, we will analytically derive the phase shift induced by each effect and numerically measure these phase shifts.

3.1 Decoupling: ϕ_{dcp}

After a mode enters the horizon ($k\eta \gtrsim 1$), the tight coupling approximation becomes less reliable, and the small decoupling effect induces both diffusion damping and phase shift to the evolution of photon perturbations. The diffusion damping was analytically studied in (e.g. Silk 1968; Hu & Sugiyama 1994; Zaldarriaga & Harari 1995) by expanding the correction to tight coupling approximation to $O(k/\dot{\tau})^2$. For our purpose of exploring the phase shift induced by decoupling, we extend the correction to $O(k/\dot{\tau})^3$ and find the analytic expression of the phase shift induced by decoupling ϕ_{dcp} (see Appendix A). Consequently, the intervals $\Delta(kr_s(\eta_p)) \equiv kr_s(\eta_p) - kr_s(\eta_{p-1})$ of the p -th and $(p-1)$ -th extrema in $\Theta_0(k, \eta)$ are no longer equal to π . Instead, $\Delta(kr_s) = \pi - \Delta(\phi_{\text{dcp}})$. The intervals $\Delta(kr_s)$ measured from the Boltzmann code `Class` (Lesgourgues & Tram 2011; Blas et al. 2011) and obtained from the analytical result in Appendix A are shown in Fig. 2. They are in good agreement except at late time when the correction to tight coupling up to $O(k/\dot{\tau})^3$ is no longer accurate and at early time when the gravitational driving is important.

3.2 Transient: $\phi_{\text{gr},\gamma}$

Both the amplitude and the phase of the acoustic oscillation are modulated by the gravitational driving at early time when the potentials have not decayed. Following Bashinsky & Seljak (2004), we define the overdensity of photon number

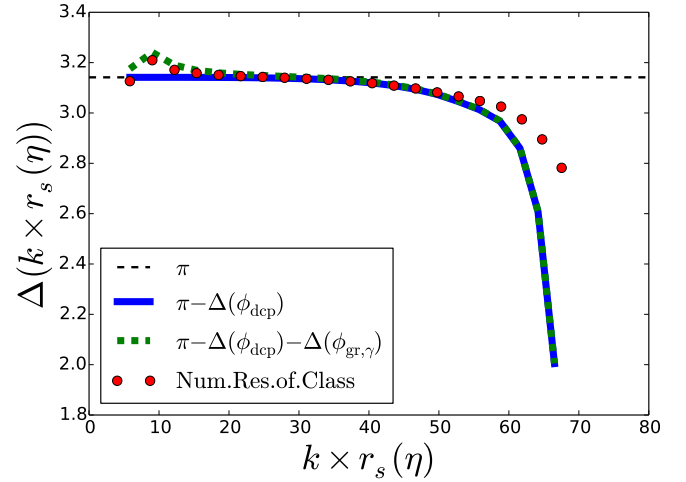


Figure 2. The intervals $\Delta(kr_s)$ of neighboring peak-trough of $[\Theta_0 + \Phi](k, \eta)$ for mode $k = 0.5 \text{ Mpc}^{-1}$. Dots are numerical results of peak-trough intervals. Solid line is the analytic result of high-order correction to the tight coupling approximation ϕ_{dcp} . Dashed line is the result of corrections from both late-time high-order correction ϕ_{dcp} and early-time gravitational driving $\phi_{\text{gr},\gamma}$ sourced by photon perturbations.

with respect to coordinate volume, $d_\gamma \equiv 3(\Theta_0 - \Psi)$ and two potentials $\Phi_\pm = \Phi \pm \Psi$, which satisfy the dynamical equation accurate to $O(k/\dot{\tau})$ [Eq. (6)],

$$d_\gamma'' + d_\gamma = -3\Phi_+, \quad (17)$$

where the prime denotes differentiation with respect to kr_s . Assuming negligible neutrinos, both Φ_\pm and d_γ can be analytically solved during radiation domination, $d_\gamma \propto \cos(kr_s + \theta(kr_s))$, where the phase shift $\theta(kr_s)$ decays with time as

$$\theta(kr_s) \simeq \frac{2}{kr_s} \Big|_{kr_s \gg 1}, \quad (18)$$

(see Appendix B for accurate expressions). We have assumed radiation domination in above derivation, so we expect it is correct only for $\eta \lesssim \eta_{\text{eq}}$. After the transition to matter domination, the gravitational potentials keep roughly constant, and θ also freezes at

$$\theta(kr_s) \Big|_{\eta > \eta_{\text{eq}}} \simeq \theta(kr_s) \Big|_{\eta = \eta_{\text{eq}}}. \quad (19)$$

The above analysis shows that, for large k , $\theta(kr_s)$ decays with time to zero, as the potentials decay to zero; while for small k , $\theta(kr_s)$ does not decay to zero, as the potentials do not completely decay. To summarize, $\theta(kr_s)$ traces the potential transient. This also explains why we call $\theta(kr_s)$ as the gravitational potential transient induced phase shift.

A minor point is that θ is the phase shift for $d_\gamma = 3(\Theta_0 - \Psi)$, while the quantity more relevant to the TT power spectrum is the effective temperature perturbation $[\Theta_0 + \Phi]$. Hence what we plot in Fig. 2 is the peak-trough spacing of $[\Theta_0 + \Phi]$, i.e., $\phi_{\text{gr},\gamma}$ instead of θ . According to Fig. 2, the transient induced phase shift $\phi_{\text{gr},\gamma}$ accounts for most of the residual phase shifts of the first few extrema in $[\Theta_0 + \Phi]$.

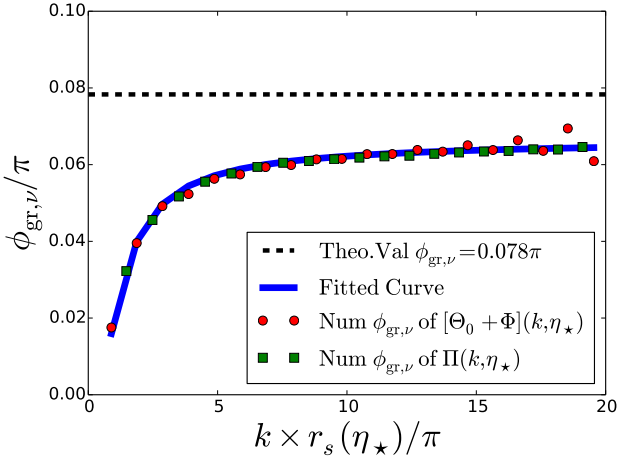


Figure 3. Phase shifts of sources induced by 3.046 neutrinos and measured at the LSS.

3.3 Neutrinos: $\phi_{\text{gr},\nu}$

Another important component during radiation domination is free-streaming neutrinos, which recast the potential transient and introduces a new phase shift component $\phi_{\text{gr},\nu}$. Under assumption of radiation domination (neglecting matter and dark energy), potential $\Phi_+(kr_s \rightarrow \infty)$ completely decays, and so does the transient induced phase shift $\phi_{\text{gr},\gamma}(kr_s \rightarrow \infty)$. More generally, previous studies (Bashinsky & Seljak 2004; Bashinsky 2007; Baumann et al. 2016) show that a nonzero phase shift $\phi_{\text{gr}}(kr_s \rightarrow \infty)$ requires modes propagating faster than the sound speed of photon-baryon plasma c_s . Neutrinos freely stream in the light speed, $c > c_s$, so a nonzero phase shift $\phi_{\text{gr},\nu}(kr_s \rightarrow \infty)$ is expected. Accurate to $O(R_\nu)$, Bashinsky & Seljak (2004) and Baumann et al. (2016) obtained a scale-independent phase shift

$$\phi_{\text{gr},\nu}(kr_s \rightarrow \infty) = 0.191R_\nu\pi, \quad (20)$$

where $R_\nu = \rho_\nu/(\rho_\nu + \rho_\gamma)$ is the energy fraction of neutrinos in the radiation. Taking account of matter domination, the above scale-independent result only applies for modes entering the horizon during radiation domination; while for modes entering the horizon during matter domination, $\phi_{\text{gr},\nu}$ approaches zero as $\sim k^2$ (see Appendix C for details).

In contrast to $\phi_{\text{gr},\gamma}$, neutrino induced phase shift $\phi_{\text{gr},\nu}$ does not the trace potential transient, though neutrinos indeed affect the transient.

4 PHASE SHIFTS IN PHOTON PERTURBATIONS AT THE LSS

In this section, we numerically measure the phase shift of photon perturbations at the LSS, single out the contribution from each effect, and analytically interpret them.

To measure the total phase shift ϕ_{tot} of the monopole source $[\Theta_0 + \Phi](kr_{s,*})$ for the fiducial cosmology, we fix $\eta = \eta_*$ and match its extrema as a function of k to those of $\cos(kr_{s,*} + \phi_{\text{tot}})$ by adjusting ϕ_{tot} . In a similar way, the

total phase shift $\phi_{\text{tot}}[\text{II}]$ of the polarization source $\Pi(kr_{s,*})$ is also measured by matching with $\sin(kr_{s,*} + \phi_{\text{tot}}[\text{II}])$.

To single out the neutrino induced phase shift $\phi_{\text{gr},\nu}$ from the total phase shift, we need to filter out the other two effects. For this purpose, we construct a comparison cosmology without neutrinos and with $z_{\text{eq}}, \theta_*, \theta_D, \omega_b$ fixed to the corresponding values of the fiducial cosmology, by adjusting the cold dark matter density ω_c , dark energy fraction Ω_Λ and the helium fraction Y_p (Follin et al. 2015). Then we measure the monopole source $[\Theta_0 + \Phi](kr_{s,*})$ at the LSS for both the fiducial cosmology and the comparison cosmology. The displacement between the extrema locations of the two is $\phi_{\text{gr},\nu}$, which is plotted in Fig. 3. As expected, $\phi_{\text{gr},\nu}$ approaches zero for small k modes and approaches a constant for large k modes. We find $\phi_{\text{gr},\nu}(k \rightarrow \infty) = 0.067\pi$, which is about 15% lower than the lowest-order analytically derived value 0.078π . Note that the $\phi_{\text{gr},\nu}$ derived in Appendix C is actually the phase shift of the monopole $\phi_{\text{gr},\nu}[\Theta_0]$, not the phase shift of the polarization $\phi_{\text{gr},\nu}[\text{II}]$. Both of them (and also $\phi_{\text{gr},\nu}[\Theta_1]$) are well fitted by

$$\phi_{\text{gr},\nu}(k, \eta_*) = \frac{1}{7.5} \tan^{-1} \left(\frac{kr_{s,*}}{\pi} - 0.5 \right), \quad (21)$$

at least for $kr_{s,*} \gtrsim \pi$.

To single out the gravitational potential transient induced phase shift $\phi_{\text{gr},\gamma}$, we solve the Einstein-Boltzmann equations in the strict tight coupling limit ($\Theta_{\ell \geq 2} = 0$) for the comparison cosmology constructed above, and evaluate the monopole at η_* . In this way, we get rid of both ϕ_{dcp} and $\phi_{\text{gr},\nu}$, therefore the only phase shift left is $\phi_{\text{gr},\gamma}$ (see left panel of Fig. 4). Analytic study [Eqs.(18,19)] shows that

$$\phi_{\text{gr},\gamma}(k, \eta_*) \simeq \frac{2}{kr_s(\eta_{\text{eq}})} \Big|_{kr_s(\eta_{\text{eq}}) \gg 1}, \quad (22)$$

which is consistent with the numerical result for large k modes (left panel of Fig. 4). The transient induced phase shift $\phi_{\text{gr},\gamma}[\text{II}]$ in the polarization source is more subtle to tap, because the polarization source $\Pi \simeq -(4k/3\bar{\tau})\Theta_1$ vanishes in the strict tight coupling limit. We tentatively extract $\phi_{\text{gr},\gamma}[\text{II}]$ by matching the extrema in $k \times \Theta_1(kr_{s,*})$ with those of $\sin(kr_{s,*} + \phi_{\text{gr},\gamma}[\text{II}])$ (see right panel of Fig. 4 for the numerical results).

With $\phi_{\text{gr},\nu}$ and $\phi_{\text{gr},\gamma}$ singled out, the residual part is certainly the decoupling induced phase shift ϕ_{dcp} given by $\phi_{\text{tot}} - (\phi_{\text{gr},\nu} + \phi_{\text{gr},\gamma})$, which as expected scales as $\sim k^3$ for small k modes (see left panel of Fig.4). The decoupling induced phase shift $\phi_{\text{dcp}}[\text{II}]$ in the polarization source is also extracted in the same way, which shows more structures than that of the monopole (see right panel of Fig.4). According to the analytic study in Appendix A, $\phi_{\text{dcp}}[\text{II}]$ scales as $\sim O(k^3) - O(k)$, where the former term is the same to ϕ_{dcp} of the monopole and the latter term comes from the fact that Π and Θ_0 are out of phase by slightly less than 90 degrees. The scaling explains the overall shape of $\phi_{\text{dcp}}[\text{II}]$. The ‘anomaly’ of the first point is due to the rise in the amplitude of Π as k increases. The polarization is sourced by the gradient of the velocity field, $\Pi \propto k\Theta_1$, and so the factor of k drives the extrema in Π to larger k modes. It is straightforward to estimate that the first extremum is driven away by $\delta(kr_s) \simeq 0.1\pi$, which is exactly the anomaly dip we observed, and the effect on other extrema is weak as their changes in k have a smaller dynamic range.

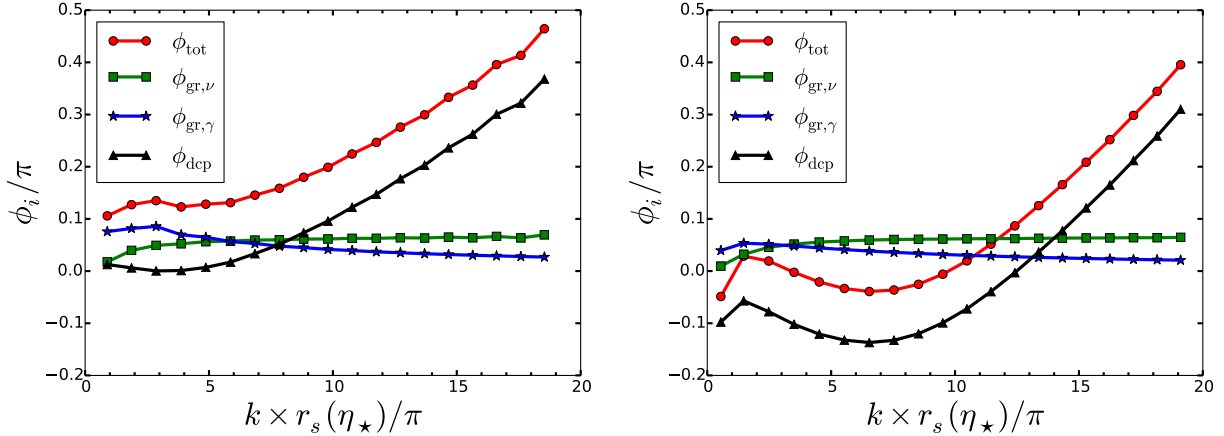


Figure 4. The phase shifts of $[\Theta_0 + \Phi]$ (left panel) and of Π (right panel) induced by different physical effects measured at the LSS.

5 PROJECTION

With our description of the phase shift ϕ_{tot} in sources at the LSS complete, we are ready to study the peak shift in the spectra. In this section, we first give a more rigorous treatment of the projection process from photon perturbations at the LSS to the power spectra, then point out the corrections to the baseline model, and measure the peak shift induced by each correction.

5.1 A Rigorous Treatment of Projection

In the baseline model, the pictorial argument of projection yields a qualitative understanding on the peak structure in the spectra. But for a quantitative understanding, we need a rigorous treatment of the projection process. Let us start from the well-known line-of-sight solutions to Eq. (2) (e.g. Hu & White 1997a; Dodelson 2003),

$$\Theta(k, \mu, \eta_0) = \int_0^{\eta_0} d\eta \tilde{S}(k, \mu, \eta) e^{ik\mu(\eta-\eta_0) - \tau(\eta)}, \quad (23)$$

where the source

$$\tilde{S}(k, \mu, \eta) = \dot{\Psi} - ik\mu\Phi - \dot{\tau} \left[\Theta_0 + \mu V_b - \frac{1}{2} P_2(\mu)\Pi \right]. \quad (24)$$

From solution Eq. (23), we obtain the multipoles

$$\begin{aligned} \Theta_\ell(k) &= \int_0^{\eta_0} d\eta g(\eta) [\Theta_0(k, \eta) + \Phi(k, \eta)] j_\ell[k(\eta_0 - \eta)] \\ &- \int_0^{\eta_0} d\eta g(\eta) \frac{iV_b}{k} \frac{d}{d\eta} j_\ell[k(\eta_0 - \eta)] \\ &+ \int_0^{\eta_0} d\eta g(\eta) \frac{3}{4} \frac{\Pi}{k^2} \frac{d^2}{d\eta^2} j_\ell[k(\eta_0 - \eta)] \\ &+ \int_0^{\eta_0} d\eta e^{-\tau} [\dot{\Phi} + \dot{\Psi}] j_\ell[k(\eta_0 - \eta)], \end{aligned} \quad (25)$$

where $g(\eta) \equiv -\dot{\tau} e^{-\tau}$ is the visibility function which narrowly peaks at the LSS $\eta = \eta_*$, $\Theta_0(k, \eta)$ is the amplitude we have investigated in Section 4 in detail. The above rigorous formula not only verifies the naive expectation of the baseline model, but also takes account of contributions from doppler effect (dipole), polarization, and integrated Sachs-Wolfe (ISW) effect. In addition, $j_\ell[k(\eta_0 - \eta)]$ is nearly zero

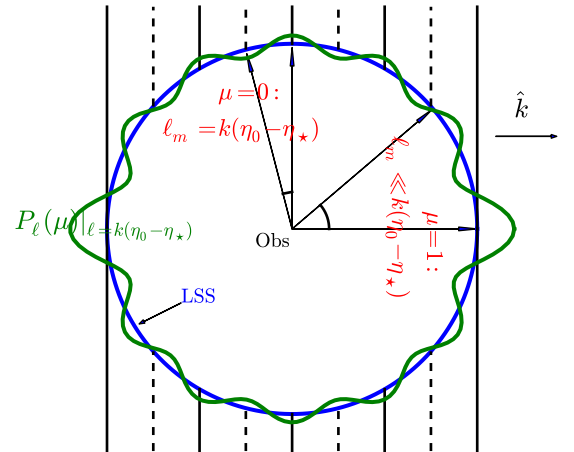


Figure 5. Illustration of the projection from three to two dimensions. The round circle is the LSS, the vertical solid (dashed) lines are the peaks (troughs) of mode \vec{k} at η_* . The wiggling curve around the LSS is a Legendre polynomial $P_\ell(\mu)$ with $\ell = k(\eta_0 - \eta_*)$, where $\mu = \hat{k} \cdot \hat{\gamma}$, is the cosine of the angle subtended by the wavevector \vec{k} and the direction of observation $\hat{\gamma}$. In the $\mu = 0$ direction, the peak-trough separation of the \vec{k} mode matches that of $P_{\ell_m}(\mu)|_{\ell_m = k(\eta_0 - \eta_*)}$ (shown). In the $\mu = 1$ direction, the peak-trough separation of the \vec{k} mode matches that of $P_{\ell_m}(\mu)|_{\ell_m \ll k(\eta_0 - \eta_*)}$ (not shown).

for $k(\eta_0 - \eta) \lesssim \ell$. The asymmetric projection can be understood with the following pictorial argument.

As shown in Fig. 5, in the direction perpendicular to the wavevector, $\mu = 0$, the peak-trough separation of the k mode matches that of $P_{\ell_m}(\mu)$ with $\ell_m = k(\eta_0 - \eta_*)$. Whereas in the direction parallel to the wavevector, $\mu = 1$, the peak-trough separation subtends a larger angle and so is better matched with a $P_{\ell_m}(\mu)$ with $\ell_m \ll k(\eta_0 - \eta_*)$. Therefore mode k distributes its power on all modes satisfying $\ell \lesssim k(\eta_0 - \eta_*)$.

In other words, the power of mode ℓ is contributed by all modes satisfying $k(\eta_0 - \eta_\star) \gtrsim \ell$ (e.g. [Hu & White 1997a](#)).

Using the transfer function $\Delta_\ell(k)$ defined by $\Delta_\ell(k) \equiv \Theta_\ell(k)/\Phi(k, 0)$ and the primordial potential power spectrum $P(k)$ defined by

$$\langle \Phi(\vec{k}, 0)\Phi^*(\vec{k}', 0) \rangle = (2\pi)^3 \delta^{(3)}(\vec{k} - \vec{k}') P(k), \quad (26)$$

C_ℓ^{TT} is written as

$$C_\ell^{\text{TT}} = \int dk k^2 P(k) \Delta_\ell^2(k), \quad (27)$$

up to some constant factor (e.g. [Seljak & Zaldarriaga 1996](#); [Dodson 2003](#)).

5.2 Corrections to the Baseline Model

In the baseline model, we simplify the monopole to be purely cosine, $[\Theta_0 + \Phi] \propto \cos(kr_s)$, simplify the LSS to be infinitely thin, i.e. $g(\eta) = \delta(\eta - \eta_\star)$, and simplify the projection from k modes to ℓ modes as one-to-one, $\ell = k(\eta_0 - \eta_\star)$. In fact, all above simplifications are not exactly correct. The phase shift ϕ_{tot} of multipoles Θ_ℓ , the finite width of the LSS and the fact that the projection from k modes to ℓ modes is not one-to-one, introduce peak shifts to the spectra. In addition, dipole Θ_1 , polarization Π and ISW effect also contribute a sub-dominant part to the power spectra. Taking TT as an example, we define the total peak shift relative to the prediction of the baseline model, $\delta\ell_p \equiv 302 p - \ell_p(\text{TT})$, where $\ell_p(\text{TT})$ is the location of p -th peak in the theoretical temperature power spectrum D_ℓ^{TT} of the fiducial cosmology (Fig. 1). In the remainder of this section, we shall investigate each correction contributing to the total peak shift $\delta\ell_p$ individually. Note that a positive $\delta\ell_p$ denotes a shift to smaller ℓ .

5.2.1 Phase Shifts in Sources: $\delta\ell[\phi_{\text{tot}}]$

The phase shift ϕ_{tot} in the monopole $[\Theta_0 + \Phi]$ at the LSS induces a peak shift in TT, $\delta\ell[\phi_{\text{tot}}] = \phi_{\text{tot}}/\theta_\star$, which is decomposed into three components $\delta\ell[\phi_{\text{gr}, \nu}] + \delta\ell[\phi_{\text{gr}, \gamma}] + \delta\ell[\phi_{\text{dcp}}]$ (Table 1 and Fig. 4). Similar analysis is also done for EE (Table 2 and Fig. 4) and TE (Table 3). We choose not to do the decomposition for TE, whose source $[\Theta_0 + \Phi] \times \Pi$ is not an independent quantity.

5.2.2 Primordial Power Spectrum: $\delta\ell[k^2 P(k)]$

Each k mode carries different amount of power which is specified by the primordial power spectrum $P(k)$, a detail not included in the baseline model. In fact, the temperature power spectrum D_ℓ^{TT} is modulated by the primordial power spectrum $P(k)$ as follows,

$$D_\ell^{\text{TT}} \simeq k^2 P(k) \sim \frac{1}{\ell}, \quad (28)$$

where we have used the scale-invariant primordial power spectrum $k^2 P(k) \sim k^{-1}$, and the simplified correspondence $\ell = k(\eta_0 - \eta_\star)$.

The modulation of the primordial power can be derived in a more rigorous way. Using Limber approximation ([Limber 1953](#); [Loverde & Afshordi 2008](#); [Lesgourgues & Tram](#)

2014),

$$\int_0^\infty dx f(x) j_\ell(x) \simeq f(L) \sqrt{\frac{\pi}{2L}}, \quad (29)$$

where $L = \ell + 1/2$, the transfer function is written as

$$\Delta_\ell(k) = \frac{1}{k} \sqrt{\frac{\pi}{2L}} g(\eta) \left[\frac{\Theta_0(k, \eta) + \Phi(k, \eta)}{\Phi(k, 0)} \right] \Bigg|_{k(\eta_0 - \eta) = L}, \quad (30)$$

and the temperature power spectrum is simplified as

$$D_\ell^{\text{TT}} = \int_0^{\eta_0} d\eta k^2 P(k) g^2(\eta) \times \left[\frac{\Theta_0(k, \eta) + \Phi(k, \eta)}{\Phi(k, 0)} \right]^2 \Bigg|_{k=L/(\eta_0 - \eta)}, \quad (31)$$

where we have used the definition (27), and changed the integration variable from k to η . Taking a step further, using facts that the visibility function is narrowly peaked at η_\star and $[\Theta_0 + \Phi](k, \eta_\star)/\Phi(k, 0) \propto \cos(kr_{s, \star} + \phi_{\text{tot}})$, we have

$$D_\ell^{\text{TT}}[j = \delta, g = \delta] \propto \frac{\cos^2(\ell\theta_\star + \phi_{\text{tot}})}{\ell}, \quad (32)$$

where $D_\ell^{\text{TT}}[j = \delta, g = \delta]$ denotes the approximate power spectrum calculated using the Limber approximation and instantaneous recombination.

The modulation by the primordial power $k^2 P(k) \sim 1/\ell$ drives the TT peaks to smaller ℓ from the predictions of the baseline model. Analytically, it is straightforward to obtain

$$\delta\ell[k^2 P(k)] \simeq \frac{1}{2\theta_\star(p\pi - \phi_{\text{tot}})} \simeq \frac{48}{p\pi - \phi_{\text{tot}}}, \quad (33)$$

which is consistent with numerical results (see Table 1). Similar analysis is also done for EE and TE.

5.2.3 Asymmetric Projection: $\delta\ell[j_\ell]$

Assuming the monopole $[\Theta_0 + \Phi](k, \eta_\star)$ peaks at k_p , the baseline model predict a peak in the power spectrum at $\ell_p = k_p(\eta_0 - \eta_\star)$. But the projection from k modes to ℓ modes is not one-to-one, instead all k modes $k \gtrsim \ell/(\eta_0 - \eta_\star)$ contribute to ℓ , and modes $k \lesssim \ell/(\eta_0 - \eta_\star)$ contribute no power to ℓ (Fig.5 and Eq.(13)). As a result, a slightly smaller ℓ (than ℓ_p) receives power from a wider range of k modes around k_p . Therefore the asymmetric projection drives TT peaks to smaller ℓ from the baseline model predicted peak locations.

The k modes and ℓ modes are connected by the transfer function $\Delta_\ell(k)$ [Eq.(25)], which is simplified as

$$\Delta_\ell(k) \simeq j_\ell(k(\eta_0 - \eta_\star)) \times \left[\frac{\Theta_0(k, \eta_\star) + \Phi(k, \eta_\star)}{\Phi(k, 0)} \right], \quad (34)$$

under the approximation of $g(\eta) = \delta(\eta - \eta_\star)$. Quantitatively, we compute an approximate spectrum $D_\ell^{\text{TT}}[g = \delta]$ from Eqs.(27, 34), and numerically measure $\delta\ell[j_\ell]$ from differences between the peak locations of $D_\ell^{\text{TT}}[j = \delta, g = \delta]$ and $D_\ell^{\text{TT}}[g = \delta]$ (see Table 1). Similar analysis is also done for EE and TE power.

According to Table 1, 2 and 3, the asymmetric projection drives the peaks in the spectra to smaller ℓ except the first EE peak. The anomaly also comes from the rise in the amplitude of Π as k increases. The first peak in Π is tiny

Table 1. The shift of the p -th peak in the temperature power spectrum D_ℓ^{TT} defined by $\delta\ell_p \equiv 302p - \ell_p(\text{TT})$, consists of $\delta\ell_{\text{monopole}}$, $\delta\ell_{\text{non-monopole}}$ and $\delta\ell_{\text{lensing}}$, where the former can be decomposed as $\delta\ell_{\text{monopole}} = \delta\ell[\phi_{\text{gr},\nu}] + \delta\ell[\phi_{\text{gr},\gamma}] + \delta\ell[\phi_{\text{dcp}}] + \delta\ell[k^2P(k)] + \delta\ell[j_\ell] + \delta\ell[g(\eta)]$.

p -th peak	$\delta\ell[\phi_{\text{gr},\nu}]$	$\delta\ell[\phi_{\text{gr},\gamma}]$	$\delta\ell[\phi_{\text{dcp}}]$	$\delta\ell[k^2P(k)]$	$\delta\ell[j_\ell]$	$\delta\ell[g(\eta)]$	$\delta\ell_{\text{monopole}}$	$\delta\ell_{\text{non-monopole}}$	$\delta\ell_{\text{lensing}}$	$\delta\ell_p$
1st	5	23	4	20	19	7	78	4	0	82 = 302 - 220
2nd	12	25	1	7	29	9	83	-16	1	68 = 604 - 536
3rd	15	26	0	6	43	7	97	-6	2	93 = 906 - 813
4th	16	21	0	4	40	3	84	-6	3	81 = 1208 - 1127
5th	17	20	2	3	45	-1	86	-3	6	89 = 1510 - 1421
6th	17	17	6	3	39	-9	73	-1	15	87 = 1812 - 1725

Table 2. The shift of the p -th peak in the polarization power spectrum D_ℓ^{EE} defined by $\delta\ell_p \equiv 302(p - 0.5) - \ell_p(\text{EE})$, consists of $\delta\ell_\Pi$ and $\delta\ell_{\text{lensing}}$, where the former is decomposed as $\delta\ell_\Pi = \delta\ell[\phi_{\text{gr},\nu}] + \delta\ell[\phi_{\text{gr},\gamma}] + \delta\ell[\phi_{\text{dcp}}] + \delta\ell[k^2P(k)] + \delta\ell[j_\ell] + \delta\ell[g(\eta)]$.

p -th peak	$\delta\ell[\phi_{\text{gr},\nu}]$	$\delta\ell[\phi_{\text{gr},\gamma}]$	$\delta\ell[\phi_{\text{dcp}}]$	$\delta\ell[k^2P(k)]$	$\delta\ell[j_\ell]$	$\delta\ell[g(\eta)]$	$\delta\ell_\Pi$	$\delta\ell_{\text{lensing}}$	$\delta\ell_p$
1st	3	12	-30	15	-4	15	11	0	11 = 151 - 140
2nd	10	16	-17	11	19	19	58	0	58 = 453 - 395
3rd	14	15	-23	6	34	21	67	0	67 = 755 - 688
4th	16	14	-31	4	43	20	66	1	67 = 1057 - 990
5th	17	13	-36	3	46	16	59	1	60 = 1359 - 1299
6th	17	12	-39	2	48	11	51	2	53 = 1661 - 1608

Table 3. The shift of the p -th peak in the power spectrum D_ℓ^{TE} is defined by $\delta\ell_p \equiv 151(p + 0.5) - \ell_p(\text{TE})$, and notations used here are similar to those in Table 1.

p -th peak	$\delta\ell[\phi_{\text{tot}}]$	$\delta\ell[k^2P(k)]$	$\delta\ell[j_\ell]$	$\delta\ell[g(\eta)]$	$\delta\ell_{\text{monopole}}$	$\delta\ell_{\text{non-monopole}}$	$\delta\ell_{\text{lensing}}$	$\delta\ell_p$
1st	32	11	21	7	71	4	0	75 = 227 - 152
2nd	27	8	28	8	71	-2	0	69 = 378 - 309
3rd	23	5	28	11	67	-6	0	61 = 529 - 468
4th	32	4	41	10	87	-3	1	85 = 680 - 595
5th	28	4	40	13	85	-3	1	83 = 831 - 748
6th	19	2	41	11	73	-5	0	68 = 982 - 914
7th	15	3	39	9	66	-5	0	61 = 1133 - 1072
8th	18	2	41	8	69	-5	0	64 = 1284 - 1220
9th	16	2	45	6	69	-5	1	65 = 1435 - 1370
10th	11	1	34	8	54	-6	0	48 = 1586 - 1538
11th	11	1	41	-4	49	-5	0	44 = 1737 - 1693
12th	13	0	28	-6	45	-7	0	38 = 1888 - 1850

compared to following few peaks. As a result, the first EE peak gains more power from larger k modes of Π , therefore is driven to larger ℓ (negative $\delta\ell$).

5.2.4 Visibility Function: $\delta\ell[g(\eta)]$

Due to the finite width of the visibility function $g(\eta)$, D_ℓ^{TT} is powered by the source $g(\eta)[\Theta_0(k, \eta) + \Phi(k, \eta)]$ from a time interval instead of a single time slice η_* . The visibility function $g(\eta)$ is positively skewed (Fig. 6). But $[\Theta_0 + \Phi](k, \eta)$ decreases in amplitude over time due to diffusion damping, so is negatively skewed. In addition, the monopole $[\Theta_0 + \Phi](k, \eta) \propto \cos(kr_s(\eta) + \phi_{\text{tot}})$ peaks at smaller k modes at later time (larger $r_s(\eta)$). Therefore the first few TT peaks would be driven to smaller ℓ , where the damping is small and the asymmetry of $g(\eta)$ dominates; and other TT peaks would be driven to large ℓ , where the asymmetry of $[\Theta_0 + \Phi](k, \eta)$ dominates due to stronger damping.

For polarization, the source term Π increases in amplitude over time, generated by free streaming. Consequently, $\Pi(\eta)$ has similar asymmetry to the visibility $g(\eta)$, and so EE and TE peaks are driven to even smaller ℓ .

Quantitatively, the phase shift induced by the visibility function $\delta\ell[g(\eta)]$ is obtained by the differences between peak locations of true D_ℓ^{TT} and of $D_\ell^{\text{TT}}[g = \delta]$. The numerical results are consistent with our qualitative analysis (Table 1, 2 and 3).

5.2.5 ISW, Dipole, Polarization: $\delta\ell[\text{non-monopole}]$

The TT and TE power spectra also receive contributions from other components: dipole Θ_1 , polarization source Π , and ISW effect $\Phi + \Psi$ (see Fig. 7 for the decomposition of TT).

The early ISW power peaks near the particle horizon scale of decoupling, which is larger than the sound horizon so

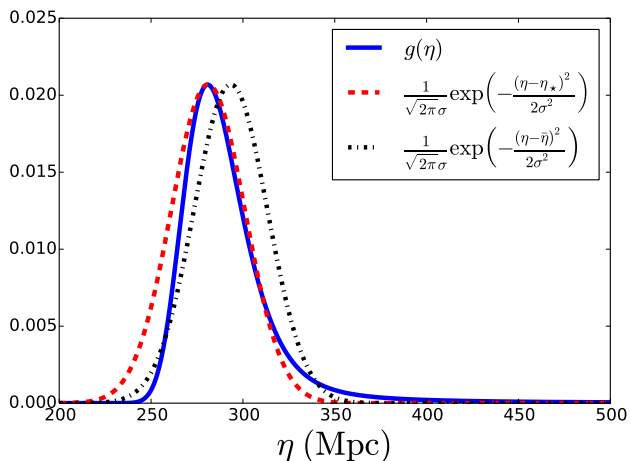


Figure 6. The comparison between the asymmetric visibility function $g(\eta)$ and two Gaussian functions both with $\sigma = 20$ Mpc, peaking at $\eta_* = 281$ Mpc and $\bar{\eta} = 293$ Mpc, respectively, where $\bar{\eta}$ is the mean decoupling time defined by $\bar{\eta} = \int g(\eta)\eta d\eta / \int g(\eta) d\eta$.

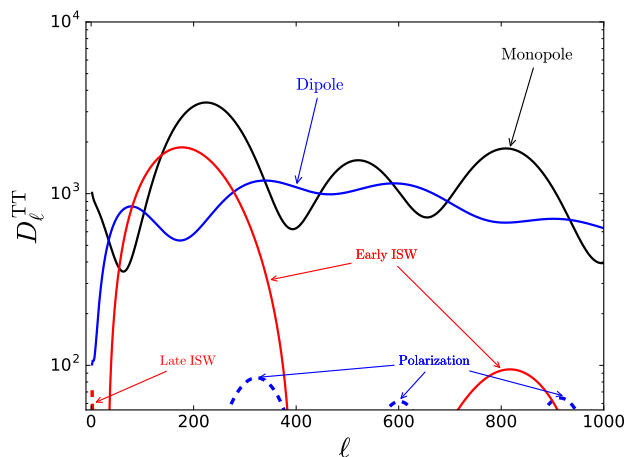


Figure 7. The contribution to the unlensed D_ℓ^{TT} from each component: dominant monopole, subdominant dipole and early ISW, and negligible polarization and late ISW.

drives the first peak to lower ℓ . The late ISW only operates at very large scale ($\ell \lesssim 10$), therefore has almost no impact on the peak locations (Hu & Sugiyama 1995).

According to the baseline model, Θ_1 is expected to be 90 degrees out of phase with Θ_0 , in which case Θ_1 would have no influence on the peak locations. Taking the decoupling effect into account, Θ_1 and Θ_0 are found to be out of phase by more than 90 degrees (see Appendix A). As a result, Θ_1 drives the peaks to larger ℓ . The impact of Π is negligible.

To summarize, $\delta\ell[\text{non-monopole}]$ of TT and TE are positive at small ℓ modes where the (early) ISW dominates, and are negative at large ℓ modes where Θ_1 dominates (see Fig. 7, Table 1 and 3).

5.2.6 Lensing: $\delta\ell[\text{lensing}]$

Gravitational lensing tends to smooth the power spectra by redistributing the power among ℓ modes (see the review of weak lensing by (Lewis & Challinor 2006)). The net effect is that peaks lose power and troughs gain power. If a peak is symmetric, the modes on both sides of the peak would lose the same amount of power, thus the peak amplitude is suppressed with the peak location unaffected. If a peak is asymmetric due to more damping at larger ℓ modes, the modes on the right side of the peak would lose more power than modes on the left side, therefore the peak is driven to smaller ℓ . The EE and TE peaks are more symmetric than TT peaks; as a result, the lensing driven phase shifts in EE and TE are smaller (see Table 1 and Table 2, 3 for comparison).

6 COMPARISON OF PREDICTED AND MEASURED PEAK LOCATIONS

In contrast to theoretical power spectra, it is impossible to directly read the peak locations out of data points in the presence of noise. To measure the peak locations from the data points, a fitting procedure is required. Taking the TT power spectrum as an example, the *Planck* collaboration (Planck Collaboration XIII 2015) first removed the damping tail, and then fit Gaussian functions to the peaks in D_ℓ^{TT} .² The peak locations measured in this specific procedure cannot be compared with the literal peak locations in the theoretical power spectrum of the fiducial cosmology. To compare the Λ CDM model predictions with the peak location measurements, we apply the same fitting procedure on the theoretical spectrum of the fiducial cosmology (Table 6). We find that peak locations measured from the data points and from the theoretical spectra are in agreement. Most of the relative displacements are within 1σ , and all the relative displacements are less than 3σ .

7 CONCLUSIONS

The acoustic peak locations of the angular power spectra have been studied in detail. We start from a baseline model, which assumes tight coupling between photons and baryons before instantaneous recombination, and a simplified one-to-one projection from k modes of the photon perturbations at the LSS to the ℓ modes of the angular power spectra. Taking the temperature power spectrum as an example, the baseline model predict that $[\Theta_0 + \Phi](k, \eta) \propto \cos(kr_s(\eta))$ and $D_\ell^{\text{TT}} \propto \cos^2(kr_{s,*})|_{\ell=k(\eta_0-\eta_*)} = \cos^2(\ell\theta_*)$, which peaks at $\ell_p^0 = p\pi/\theta_* = 302 p$. The baseline model is roughly correct in its prediction for the peak spacing and for the relative positions of the peaks in different spectra, but is off by a large margin in its absolute predictions of peak locations. For example, the first peak in D_ℓ^{TT} is at $\ell_1 = 220$, which is shifted by $\delta\ell_1 = 82$ from the baseline model prediction $\ell_1^0 = 302$. The shift of the true power spectra locations relative to the baseline model predictions comes both from the phase shift

² Different fitting procedures were also investigated in previous works (e.g. Aghamousa et al. 2012, 2015).

Table 4. Locations of the peaks in the power spectra. The peak locations measured from the *Planck* 2015 data are listed in the 3rd column (Table E.2. in [Planck Collaboration XIII 2015](#)), and the peak locations predicated by the fiducial cosmology are listed in the 2nd column (Note that these peak locations are determined by the fitting procedure used on the data, therefore are different from the literal peak locations of theoretical power spectra).

<i>p</i> -th peak	multipole (model)	multipole (data)
TT power spectrum		
1st	220.9	220.0 ± 0.5
2nd	538.5	537.5 ± 0.7
3rd	809.5	810.8 ± 0.7
4th	1122.5	1120.9 ± 1.0
5th	1445.7	1444.2 ± 1.1
6th	1774	1776 ± 5
7th	2071	2081 ± 25
8th	2429	2395 ± 24
EE power spectrum		
1st	135.3	137 ± 6
2nd	395.4	397.2 ± 0.5
3rd	689.7	690.8 ± 0.6
4th	992.1	992.1 ± 1.3
5th	1299	1296 ± 4
TE power spectrum		
1st	149.0	150.0 ± 0.8
2nd	307.8	308.5 ± 0.4
3rd	471.3	471.2 ± 0.4
4th	593.4	595.3 ± 0.7
5th	747.3	746.7 ± 0.6
6th	915.9	916.9 ± 0.5
7th	1073.3	1070.4 ± 1.0
8th	1224.8	1224.0 ± 1.0
9th	1371.9	1371.7 ± 1.2
10th	1542.1	1536.0 ± 2.8
11th	1700.6	1693.0 ± 3.3
12th	1865	1861 ± 4

ϕ_{tot} in the acoustic oscillations of the photon perturbations $[\Theta_0 + \Phi](k, \eta) \propto \cos(kr_s(\eta) + \phi_{\text{tot}})$, and the fact that the projection from photon perturbations at the LSS to the angular power spectra is far more complicated than assumed in the baseline model.

The phase shift $\phi_{\text{tot}}(k, \eta_*)$ consists of two components ϕ_{dcp} and ϕ_{gr} , where ϕ_{dcp} is the phase shift induced by decoupling and dominates for large k modes ($k\eta_* \gtrsim 1$), and ϕ_{gr} is the phase shift induced by the gravitational driving and dominates for small k modes ($k\eta_* \lesssim 1$). The latter component can be further decomposed as $\phi_{\text{gr},\gamma} + \phi_{\text{gr},\nu}$, where $\phi_{\text{gr},\gamma}$ is the transient induced phase shift and $\phi_{\text{gr},\nu}$ is the neutrino induced phase shift. A key difference between the two is that $\phi_{\text{gr},\gamma}$ decays with increasing k , while $\phi_{\text{gr},\nu}$ grows with increasing k and approaches a nonzero constant. This difference stems from the time dependence of these effects, and the fact that at higher k there is more time, in units of the natural period of the oscillator $2\pi/(kr_s)$, between horizon-crossing and matter-radiation equality.

The projection from k modes to ℓ modes is not one-to-one as assumed in the baseline model. All perturbation modes satisfying $k \gtrsim \ell/(\eta_0 - \eta_*)$ contribute to the angular power spectra at a given ℓ . In addition, the LSS has non-zero width. Both of these differences with the baseline model introduce peak shifts to the power spectra. Other effects including the modulation of the primordial power spectrum $P(k)$, (early) ISW effect, dipole moment of photon perturbation and lensing also contribute subdominant shifts to the peak locations.

We also compare each peak location determined from *Planck* measurements to the location predicted under the assumption of the best-fit Λ CDM model, and find consistency.

Our entire motivation in pursuing this work was to achieve an understanding of the numerically calculated predictions of the Λ CDM model. However, we now speculate on a potential application. With further development, perhaps our analytic understanding of the shifts in the peak locations could be combined with the morphing procedure of [Sigurdson \(2000\)](#), to achieve a highly accurate, very fast, Boltzmann code emulator, improving upon interpolative schemes such as PICO ([Fendt & Wandelt 2007](#)).

8 ACKNOWLEDGEMENTS

We thank the anonymous referee for his/her valuable comments and suggestions, including the suggestion that there might be an application to Boltzmann code emulation. We also thank Douglas Scott for careful reading this manuscript and introducing the history of first TT peak detection. This work made extensive use of the NASA Astrophysics Data System and of the `astro-ph` preprint archive at [arXiv.org](#). All the numerical calculations are done with the Boltzmann code `Class`.

APPENDIX A: ϕ_{dcp}

High-order corrections to the tight coupling approximation are only important at late time after a mode enters the horizon ($k\eta \gtrsim 1$), and the gravitational potentials have decayed. Following [Zaldarriaga & Harari \(1995\)](#), we set $\Phi = 0$ and $\Psi = 0$ in this subsection (Refer to [Blas et al. \(2011\)](#) for rigorous high-order correction to the tight coupling approximation). Assuming the formal solutions

$$\Theta_i, \Theta_{p,i}, V_b \sim e^{i \int \omega d\eta}, \quad (\text{A1})$$

the dipole moment of Eq.(2) is written as

$$\Theta_1 - \frac{i}{3}V_b = \frac{1}{\dot{\tau}} \left[i\omega\Theta_1 + k \left(\frac{2}{3}\Theta_2 - \frac{1}{3}\Theta_0 \right) \right]. \quad (\text{A2})$$

Accurate to $O(k/\dot{\tau})^3$ on both sides of the above equation, Eqs.(2, 3) are decomposed as

$$\begin{aligned} \Theta_0 &= \frac{ik}{\omega}\Theta_1, \\ \Theta_2 &= -\frac{8}{15}\frac{k}{\dot{\tau}}\Theta_1 \left(1 + \frac{11}{6}\frac{i\omega}{\dot{\tau}} \right), \\ \Pi &= \frac{5}{2}\Theta_2 \left(1 + \frac{3}{2}\frac{i\omega}{\dot{\tau}} \right), \end{aligned} \quad (\text{A3})$$

and Eq.(4) is expanded as

$$\Theta_1 - \frac{i}{3}V_b = \Theta_1 \left[-i\frac{\omega R_b}{\dot{\tau}} + \left(\frac{\omega R_b}{\dot{\tau}}\right)^2 + i\left(\frac{\omega R_b}{\dot{\tau}}\right)^3 \right], \quad (\text{A4})$$

where we have dropped a term $\frac{R_b}{\dot{\tau}}\frac{\dot{a}}{a}$ in the bracket on the right-hand side, which is smaller than $\frac{R_b}{\dot{\tau}}\omega$ when the mode is within the horizon $k\eta > 1$.

Plugging Eqs.(A3,A4) into Eq.(A2), we obtain, for $\omega = \omega_0 + \delta\omega_0 + i\gamma$,

$$\begin{aligned} \omega_0 &= kc_s, & \frac{\gamma}{\omega_0} &= -\frac{k}{\dot{\tau}} \frac{(c_s^2 R_b^2 + \frac{16}{45})}{2c_s(1 + R_b)}, \\ \frac{\delta\omega_0}{\omega_0} &= \frac{k^2}{\dot{\tau}^2} \frac{(c_s^2 R_b^2 + \frac{88}{135}) - \frac{3}{4}(c_s^2 R_b^2 + \frac{16}{45})(5c_s^2 R_b^2 + \frac{16}{45})}{2(1 + R_b)}. \end{aligned} \quad (\text{A5})$$

Note that $\dot{\tau}$ is negative, and so γ is positive. Therefore, accurate to $O(k/\dot{\tau})^3$, $\Theta_0(k, \eta)$ can be described as a damped oscillator with a time-dependent phase shift, i.e.

$$\Theta_0(k, \eta) \propto \cos(kr_s + \phi_{\text{dcp}})e^{-k^2/k_D^2}, \quad (\text{A6})$$

where

$$\begin{aligned} \phi_{\text{dcp}} &= \int \delta\omega_0 d\eta \sim O(k/\dot{\tau})^2, \\ k^2/k_D^2 &= \int \gamma d\eta \sim O(k/\dot{\tau}). \end{aligned} \quad (\text{A7})$$

Other useful multipoles obtained are

$$\begin{aligned} \Theta_1 &\propto c_s \sin(kr_s + \phi_{\text{dcp}} + \phi_1)e^{-k^2/k_D^2}, \\ \Pi &\propto -\frac{4k}{3\dot{\tau}}c_s \sin(kr_s + \phi_{\text{dcp}} + \phi_2)e^{-k^2/k_D^2}, \end{aligned} \quad (\text{A8})$$

where

$$\phi_1 = \tan^{-1}\left(\frac{\gamma}{\omega_0}\right), \quad \phi_2 = -\tan^{-1}\left(\frac{21\gamma}{4\omega_0}\right), \quad (\text{A9})$$

and $\phi_1(\phi_2)$ comes from the fact that $\Theta_1(\Pi)$ and Θ_0 are not exactly 90 degrees out of phase due to the diffusion damping.

APPENDIX B: $\phi_{\text{gr},\gamma}$

The solution to the equation of the forced oscillator [Eq.(17)] is written as (e.g. Eq. (8.24) of Dodelson (2003))

$$\begin{aligned} d_\gamma(kr_s) &= d_\gamma(0) \cos(kr_s) \\ &\quad - 3 \int_0^{kr_s} d(kr'_s) \Phi_+(kr'_s) \sin(kr_s - kr'_s), \end{aligned} \quad (\text{B1})$$

which can be simplified as

$$\begin{aligned} d_\gamma(kr_s) &= [d_\gamma(0) + 3A(kr_s)] \cos(kr_s) - 3B(kr_s) \sin(kr_s), \\ &= \sqrt{[d_\gamma(0) + 3A]^2 + (3B)^2} \cos(kr_s + \theta), \end{aligned} \quad (\text{B2})$$

where $d_\gamma(0)$ is the initial amplitude denoted as $d_\gamma(0) \equiv -3\zeta$, and

$$\begin{aligned} A(kr_s) &= \int_0^{kr_s} \Phi_+(kr'_s) \sin(kr'_s) d(kr'_s), \\ B(kr_s) &= \int_0^{kr_s} \Phi_+(kr'_s) \cos(kr'_s) d(kr'_s), \end{aligned} \quad (\text{B3})$$

$$\theta = \sin^{-1}\left(\frac{3B}{\sqrt{(3A + d_\gamma(0))^2 + (3B)^2}}\right). \quad (\text{B4})$$

To solve A and B , Φ_+ is required. In the radiation domination, Φ_+ is sourced by Φ_- (e.g. Eq.(2.50) of Baumann et al. (2016))

$$\Phi_+'' + \frac{4}{kr_s}\Phi_+' + \Phi_+ = S(\Phi_-) \equiv \Phi_-'' + \frac{2}{kr_s}\Phi_-' + 3\Phi_-, \quad (\text{B5})$$

and Φ_- is sourced by the radiation stress which is dominated by free-streaming neutrinos (e.g. Eq.(5.33) of Dodelson (2003))

$$k^2\Phi_- = -32\pi G a^2 \rho_\nu \mathcal{N}_2, \quad (\text{B6})$$

where we have dropped the negligible stress of photons.

Assuming a cosmology without neutrinos, or accurate to $O(R_\nu^0)$, where R_ν is the energy fraction of neutrinos in radiation, $R_\nu \equiv \rho_\nu/(\rho_\nu + \rho_\gamma)$, we have $\Phi_-^{(0)} = 0$, and $\Phi_+^{(0)}$ can be analytically solved as

$$\Phi_+^{(0)}(kr_s) = -4\zeta \frac{\sin(kr_s) - kr_s \cos(kr_s)}{(kr_s)^3}. \quad (\text{B7})$$

Consequently, A and B are integrated as

$$\begin{aligned} A^{(0)}(kr_s) &= 2\zeta \left(1 - \frac{\sin^2(kr_s)}{(kr_s)^2}\right) \xrightarrow{kr_s \rightarrow \infty} 2\zeta, \\ B^{(0)}(kr_s) &= 2\zeta \frac{kr_s - \cos(kr_s) \sin(kr_s)}{(kr_s)^2} \xrightarrow{kr_s \rightarrow \infty} 0 \end{aligned} \quad (\text{B8})$$

Plugging $A^{(0)}$ and $B^{(0)}$ into Eq.(B4), we obtain the phase shift θ for $[\Theta_0 - \Psi]$. With d_γ and $\Phi_\pm^{(0)}$ known, it is straightforward to obtain both $[\Theta_0 + \Phi]$ and its phase shift $\phi_{\text{gr},\gamma}$, which is indistinguishable from θ after the mode enters the horizon.

APPENDIX C: $\phi_{\text{gr},\nu}$

Following Baumann et al. (2016), $\phi_{\text{gr},\nu}$ can be analytically studied by a perturbation approach, whose earlier version was originally developed for probing the impact of neutrino free-streaming on tensor modes (e.g. Weinberg 2004; Dicus & Repko 2005; Watanabe & Komatsu 2006; Miao & Zhang 2007; Xia & Zhang 2008). Accurate to $O(R_\nu)$, the two potentials are written as

$$\Phi_- = R_\nu \Phi_-^{(1)}, \quad \Phi_+ = \Phi_+^{(0)} + R_\nu \Phi_+^{(1)}. \quad (\text{C1})$$

In the radiation domination, Eq.(B6) can be rewritten as

$$\Phi_- = -\frac{4}{k^2 r_s^2} R_\nu \mathcal{N}_2 = -\frac{4}{3k^2 r_s^2} R_\nu D_{\nu,2}, \quad (\text{C2})$$

where D_ν is defined by $D_\nu \equiv 3(\mathcal{N} - \Psi)$, and $D_{\nu,2}$ is the quadrupole moment, $D_{\nu,2} = 3\mathcal{N}_2$. To determine Φ_- to $O(R_\nu)$, we only need to specify $D_{\nu,2}$ to $O(R_\nu^0)$.

The evolution of neutrino perturbation is governed by (e.g. Eq.(4.107) of Dodelson (2003)),

$$\dot{D}_\nu + ik\mu D_\nu = -3ik\mu \Phi_+, \quad (\text{C3})$$

and the solution is

$$\begin{aligned} D_\nu(\eta) &= D_\nu(0)e^{-ik\mu\eta} \\ &\quad - 3ik\mu \int_0^\eta d\eta' e^{-ik\mu(\eta-\eta')} \Phi_+(\eta'), \end{aligned} \quad (\text{C4})$$

where $D_\nu(0)$ is determined by the inflation inspired initial condition $D_\nu(0) = D_{\nu,0}(0) = -3\zeta$. Plugging the zeroth-order potential $\Phi_+^{(0)}$ into the above solution, $D_\nu(\eta)$ and consequently $D_{\nu,2}$ of $O(R_\nu^0)$ are obtained.

Combining Eq.(C2) and Eq.(B5), $\Phi_-^{(1)}(kr_s)$ and $\Phi_+^{(1)}(kr_s)$ are obtained. Plugging $\Phi_+^{(1)}(kr_s)$ into Eqs.(B3), A and B can be numerically obtained, accurate to $O(R_\nu)$ (Baumann et al. 2016),

$$\begin{aligned} A(kr_s \rightarrow \infty) &= 2\zeta(1 - 0.134R_\nu), \\ B(kr_s \rightarrow \infty) &= 0.600\zeta R_\nu. \end{aligned} \quad (\text{C5})$$

Plugging A and B into Eq.(B4), the phase shift induced by neutrinos accurate to $O(R_\nu)$ is obtained

$$\phi_{\text{gr},\nu} = \frac{B}{\zeta} = 0.191R_\nu\pi. \quad (\text{C6})$$

The above $\phi_{\text{gr},\nu}$ is derived under the assumption of radiation domination, so is appropriate only for large k modes. Taking the matter domination epoch into account, $\phi_{\text{gr},\nu}$ is expected to approach zero as $\sim k^2$ for small k modes (Baumann et al. 2016).

REFERENCES

- Aghamousa A., Arjunwadkar M., Souradeep T., 2012, *The Astrophysical Journal*, 745, 114
- Aghamousa A., Shafieloo A., Arjunwadkar M., Souradeep T., 2015, *Journal of Cosmology and Astroparticle Physics*, 2015, 007
- Albrecht A., 2000, preprint ([arXiv:0009129](https://arxiv.org/abs/0009129))
- Amendola L., Gordon C., Wands D., Sasaki M., 2002, *Physical Review Letters*, 88, 211302
- Atrio-Barandela F., Doroshkevich A. G., 1994, *The Astrophysical Journal*, 420, 26
- Bartolo N., Matarrese S., Riotto A., 2007, *Journal of Cosmology and Astroparticle Physics*, 2007, 019
- Bashinsky S., 2007, preprint ([arXiv:0707.0692](https://arxiv.org/abs/0707.0692))
- Bashinsky S., Seljak U., 2004, *Physical Review D*, 69, 83002
- Baumann D., Green D., Meyers J., Wallisch B., 2016, *Journal of Cosmology and Astroparticle Physics*, 1508, 6342
- Bean R., Dunkley J., Pierpaoli E., 2006, *Physical Review D*, 74, 1
- Benoît A., et al., 2003, *Astronomy and Astrophysics*, 399, L25
- Bernardis P., et al., 2000, *Nature*, 404, 955
- Bernardis P., et al., 2002, *The Astrophysical Journal*, 564, 559
- Blas D., Lesgourgues J., Tram T., 2011, *Journal of Cosmology and Astroparticle Physics*, 7, 34
- Bond J. R., H. Jaffe A., 1999, *Philosophical Transactions of the Royal Society A*, 357, 57
- Bond J. R., Jaffe A. H., Knox L., 1998, *Physical Review D*, 57, 2117
- Bond J. R., Crittenden R. G., Jaffe A. H., Knox L., 1999, *Comput. Sci. Eng.*, 1
- Bond J. R., et al., 2000a, preprint ([arXiv:0011378](https://arxiv.org/abs/0011378))
- Bond J. R., Jaffe A. H., Knox L., 2000b, *The Astrophysical Journal*, 533, 19
- Bucher M., Moodley K., Turok N., 2001, *Physical Review Letters*, 87, 191301
- Bucher M., Moodley K., Turok N., 2002, *Physical Review D*, 66
- Cai Z., Zhang Y., 2012, *Classical and Quantum Gravity*, 29, 1
- Corasaniti P., Melchiorri A., 2008, *Physical Review D*, 77, 103507
- Dicus D. A., Repko W. W., 2005, *Physical Review D*, 72, 088302
- Dodelson S., 2003, *Modern Cosmology*. Academic Press, New York
- Doroshkevich A., Zel'Dovich Y., Syunyaev R., 1978, *Soviet Astronomy*, 22, 523
- Durrer R., Novosyadlyj B., Apunevych S., 2001, *The Astrophysical Journal*, 583, 34
- Efstathiou G., Bridle S. L., Lasenby A. N., Hobson M. P., Ellis R. S., 1999, *Monthly Notices of the Royal Astronomical Society*, 303, L47
- Fendt W. A., Wandelt B. D., 2007, *The Astrophysical Journal*, 654, 2
- Follin B., Knox L., Millea M., Pan Z., 2015, *Physical Review Letters*, 115, 91301
- Hancock S., Rocha G., Lasenby A. N., Gutierrez C. M., 1998, *Monthly Notices of the Royal Astronomical Society*, 294, L1
- Hinshaw G., et al., 2007, *The Astrophysical Journal Supplement Series*, 170, 288
- Hinshaw G., et al., 2013, *The Astrophysical Journal Supplement Series*, 208, 19
- Hu W., Dodelson S., 2002, *Annual Review of Astronomy and Astrophysics*, 40, 171
- Hu W., Sugiyama N., 1994, *The Astrophysical Journal*, 444, 31
- Hu W., Sugiyama N., 1995, *Physical Review D*, 51, 2599
- Hu W., Sugiyama N., 1996, *The Astrophysical Journal*, 471, 542
- Hu W., White M., 1996, *The Astrophysical Journal*, 471, 30
- Hu W., White M., 1997a, *Physical Review D*, 56, 596
- Hu W., White M., 1997b, *The Astrophysical Journal*, 479, 568
- Jaffe A. H., et al., 2001, *Physical Review Letters*, 86, 3475
- Jones W. C., et al., 2006, *Astrophysical Journal*, 647, 823
- Jorgensen H. E., Kotok E., Naselsky P., Novikov I., 1995, *Astronomy and Astrophysics*, 294, 639
- Knox L., Page L., 2000, *Physical Review Letters*, 85, 1366
- Komatsu E., et al., 2009, *The Astrophysical Journal Supplement Series*, 180, 330
- Komatsu E., et al., 2011, *The Astrophysical Journal Supplement Series*, 192, 18
- Lesgourgues J., Tram T., 2011, *Journal of Cosmology and Astroparticle Physics*, 9, 32
- Lesgourgues J., Tram T., 2014, *Journal of Cosmology and Astroparticle Physics*, 2014, 032
- Lewis A., Challinor A., 2006, *Physics Reports*, 429, 1
- Lewis A., Challinor A., Lasenby A., 2000, *The Astrophysical Journal*, 538, 473
- Limber D., 1953, *The Astrophysical Journal*, 117, 134
- Lineweaver C. H., Barbosa D., 1998, *The Astrophysical Journal*, 496, 624
- Loverde M., Afshordi N., 2008, *Physical Review D*, 78, 123506
- Ma C.-P., Bertschinger E., 1995, *The Astrophysical Journal*, 455, 7
- Magueijo J., Albrecht A., Ferreira P., Coulson D., 1996, *Physical Review D*, 54, 3727
- Miao H. X., Zhang Y., 2007, *Physical Review D*, 75, 104009
- Miller A. D., et al., 1999, *The Astrophysical Journal*, 524, L1
- Moodley K., Bucher M., Dunkley J., Ferreira P. G., Skordis C., 2004, *Physical Review D*, 70, 1
- Mukhanov V., 1992, *Physics Reports*, 215, 203
- Mukhanov V., 2004, *International Journal of Theoretical Physics*, 43, 623
- Naess S., et al., 2014, *Journal of Cosmology and Astroparticle Physics*, 2014, 007
- Page L., et al., 2003, *The Astrophysical Journal Supplement Series*, 148, 233
- Peebles P. J. E., Yu J. T., 1970, *The Astrophysical Journal*, 162, 815
- Pierpaoli E., 2000, *Science*, 287, 2171
- Planck Collaboration XI 2015, preprint ([arXiv:1507.02704](https://arxiv.org/abs/1507.02704))
- Planck Collaboration XIII 2015, preprint ([arXiv:1502.01589](https://arxiv.org/abs/1502.01589))
- Planck Collaboration XVI 2014, *Astronomy & Astrophysics*, 571, A16

- Planck Collaboration XXII 2014, *Astronomy & Astrophysics*, 571, A22
- Pryke C., et al., 2008, *The Astrophysical Journal*, 692, 24
- Readhead A. C. S., et al., 2004, *Science*, 306, 836
- Scott D., White M., 1994, preprint ([arXiv:9407073](#))
- Seljak U., 1994, *The Astrophysical Journal Letters*, 435, L87
- Seljak U., Zaldarriaga M., 1996, *The Astrophysical Journal*, 469, 437
- Sigurdson K., 2000, *New Astronomy*, 5, 91
- Silk J., 1968, *The Astrophysical Journal*, 151, 459
- Smoot G., Scott D., 1997, preprint ([arXiv:9711069](#))
- Tegmark M., 1999, *The Astrophysical Journal*, 514, L69
- Tegmark M., Zaldarriaga M., 2000a, *Physical review letters*, 85, 2240
- Tegmark M., Zaldarriaga M., 2000b, *The Astrophysical Journal*, 544, 30
- Tram T., Lesgourgues J., 2013, *Journal of Cosmology and Astroparticle Physics*, 2013, 002
- Trotta R., Riazuelo a., Durrer R., 2001, *Physical Review Letters*, 87, 231301
- Turok N., 1996a, *Physical Review D*, 54, R3686
- Turok N., 1996b, *Physical Review Letters*, 77, 4
- Watanabe Y., Komatsu E., 2006, *Physical Review D*, 73, 123515
- Weinberg S., 2001a, *Physical Review D*, 64, 123511
- Weinberg S., 2001b, *Physical Review D*, 64, 123512
- Weinberg S., 2002, *The Astrophysical Journal*, 581, 810
- Weinberg S., 2004, *Physical Review D*, 69, 023503
- Xia T. Y., Zhang Y., 2008, *Physical Review D*, 78, 123005
- Zaldarriaga M., Harari D. D., 1995, *Physical Review D*, 52, 3276